Hindawi Publishing Corporation
Applied Bionics and Biomechanics
Volume 2016, Article ID 6909745, 11 pages
http://dx.doi.org/10.1155/2016/6909745

Research Article

Numerical Analysis of Hydrodynamics for Bionic Oscillating Hydrofoil Based on Panel Method

Gang Xue, Yanjun Liu, Muqun Zhang, and Hongpeng Ding

Key Laboratory of High Efficiency and Clean Mechanical Manufacture, School of Mechanical Engineering, Shandong University, No. 17923, Jingshi Road, Jinan, Shandong 250061, China

Correspondence should be addressed to Yanjun Liu; lyjky111@163.com

Received 27 February 2016; Revised 22 June 2016; Accepted 30 June 2016

Academic Editor: Luis Gracia

The kinematics model based on the Slender-Body theory is proposed from the bionic movement of real fish. The Panel method is applied to the hydrodynamic performance analysis innovatively, with the Gauss-Seidel method to solve the Navier-Stokes equations additionally, to evaluate the flexible deformation of fish in swimming accurately when satisfying the boundary conditions. A physical prototype to mimic the shape of tuna is developed with the revolutionized technology of rapid prototyping manufacturing. The hydrodynamic performance for rigid oscillating hydrofoil is analyzed with the proposed method, and it shows good coherence with the cases analyzed by the commercial software *Fluent* and the experimental data from robofish. Furthermore, the hydrodynamic performance of coupled hydrofoil, which consisted of flexible fish body and rigid caudal fin, is analyzed with the proposed method. It shows that the caudal fin has great influence on trailing vortex shedding and the phase angle is the key factor on hydrodynamic performance. It is verified that the shape of trailing vortex is similar to the image of the motion curve at the trailing edge as the assumption of linear vortex plane under the condition of small downwash velocity. The numerical analysis of hydrodynamics for bionic movement based on the Panel method has certain value to reveal the fish swimming mechanism.

1. Introduction

The research on propulsion mechanism of aquatic animal has very important significance in recognizing nature and developing bionics. In almost the entire Reynolds number spectrum domain, the undulate propulsion of aquatic animal has shown decent hydrodynamic performance and the undulate motion based on flexible fish body has been proven as a high efficient propulsion method [1]. Katz and Weihs have conducted intensive researches to prove that the propulsive efficiency of flexible undulate hydrofoil was 20% higher than the rigid one, and no significant decline happened in propulsive force [2]. The experiments on undulate oscillating hydrofoil conducted by Triantafyllou et al. showed the propulsive efficiency could be about 90% under certain oscillating frequency and amplitude [3]. A kind of wire-driven robotic fish has been developed by Du et al., and the propulsive efficient could reach to 65% because of the high-flexible tail part [4]. Wang et al. also proposed a two-joint linear hypocycloid tail driving system for mimicking a real fish tail's oscillating motion [5]. However, it is difficult for present physical models to simulate the undulate motion of real fish precisely. Meanwhile, the experiments to measure hydrodynamic performance and to observe flow field structure of flexible oscillating hydrofoil are not precise enough. So the numerical analysis is an important method for studying flexible oscillating hydrofoil.

Numerical analysis method in the research of hydrodynamic performance for rigid oscillating hydrofoil has been comparatively mature. Wu et al. have studied the hydrodynamic performance of rigid oscillating hydrofoil with the standard k-ω SST turbulence model and the correction γ-Reθ transition turbulence model to discover that the hydrodynamic characteristic curve of hydrofoil had a large variation range because of the dynamic stall as a result of the separated vortices at leading edge with a large attack angle [6]. Celik et al. have studied the hydrodynamic performance of the static 2D and 3D hydrofoil with the boundary element method [7]. Zhao et al. have studied the unsteady development process of vortex near the trailing edge with the Finite-Time Lyapunov

Exponent method based on the Lagrange coordinate system [8]. Karim et al. have studied the hydrodynamic performance of rigid oscillating hydrofoil under the effect of surface wave by solving the Navier-Stokes equations with finite volume method [9]. Shi et al. have discovered that the average lift coefficient and the average drag coefficient of cascade hydrofoil were smaller than those of the single hydrofoil, as well as the reverse jet function in the wake field [10].

Besides, numerical analysis method has been applied to the research of fish-like flexible oscillating hydrofoil preliminarily and achieved some results. Zhu, Liu et al., and Zhang et al. have studied the effect of flexible caudal fin deformation in chordwise direction and spanwise direction on the hydrodynamic performance [11–13]. It was shown that deformation in spanwise direction decreased the propulsive force and propulsive efficiency while the input power of caudal fin changed along with the deformation phase angle in chordwise direction. Su et al. have discussed the effect of forward speed, traverse motion amplitude, oscillating amplitude, oscillating frequency, and phase angle on the flexible undulate propulsive performance [14]. Leroyer and Visonneau have utilized the numerical analysis method to study the hydrodynamic performance of swimming fish with the 3D flexible fish model [15, 16]. Lee et al. have studied the trailing vortex of oscillating hydrofoil with the Particle-Grid Hybrid Method and Subgrid Eddy Viscosity Model to find that the free stream cycle would affect the shape and the shedding process of trailing vortex [17]. The above researches and methods have important guiding significance on the study of bionic oscillating hydrofoil.

In this paper, the Panel method is applied to study the hydrodynamic performance of rigid oscillating hydrofoil, the NACA0012 hydrofoil, and the simulation in commercial software *Fluent* and the experimental data from physical prototype are utilized to verify the results. Furthermore, the unsteady motion of coupled hydrofoil consisted of flexible fish body and rigid caudal fin is numerically simulated in the proposed method and the wake field characteristics in different fish-like motion states are analyzed to study the effect of trailing vortex on propulsive performance and the coupling effect of the coupled hydrofoil.

2. Kinematics Model and Numerical Method

2.1. Kinematics Model. Bionic kinematics model is the foundation to numerically study hydrodynamic performance of fish-like oscillating hydrofoil. Su et al. have proposed a fish-like motion model that deformation happened from arbitrary point of fin-chord to trailing edge while no deformation happened from that point to leading edge [14]. As the famous Slender-Body theory proposed by Lighthill, transversal oscillation that happened in the anterior part of fish had little help to improve propulsive performance but to increase energy consumption and to reduce propulsive efficiency inversely [18]. Further researches have revealed that the anterior part of fish keeping still and the caudal peduncle (the backwards third of fish body) oscillating, the carangiform propulsion mode, would achieve large propulsive force and high propulsive efficiency. The two-dimensional coordinate system of swimming fish body was established with the origin at the fish head, as shown in Figure 1.

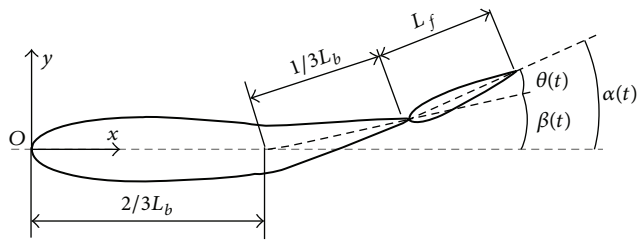

Figure 1: Coordinate for the fish motion.

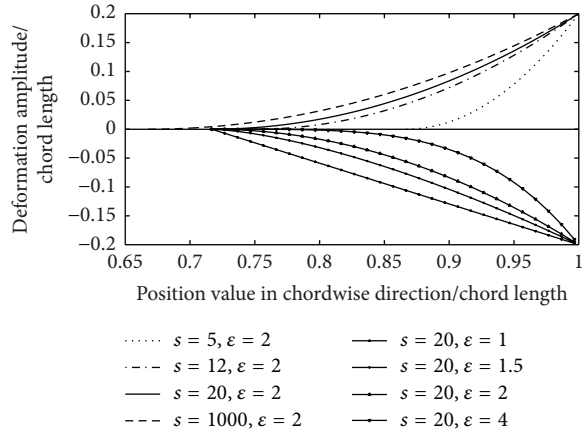

Figure 2: Deformation of caudal peduncle under various s and ε.

The caudal peduncle motion model of carangiform propulsion mode was proposed after optimizing the motion model proposed by Su et al. [14], as follows:

$$A(x,t) = A\left[\frac{s}{s-1}x - \frac{2s+3}{3(s-1)}\right]^{\varepsilon} \sin(2\pi f t) \qquad s > 3,\ \varepsilon > 1,\ \frac{2}{3} + \frac{1}{s} \le x \le 1, \tag{1}$$

where $A(x,t)$ is the amplitude of chordwise caudal peduncle deformation, f is the deformation frequency, s is the coefficient to change deformation range, and ε is the coefficient to change deformation flexibility. As the value of s is smaller, the deformation is closer to the trailing edge, and as the value of ε is larger, the initial deformation is more gentle. A is the characteristic amplitude, as follows:

$$A = \frac{A_{\max}}{L_b}\left[\frac{3(s-1)}{s-3}\right]^{\varepsilon}, \tag{2}$$

where $A_{\max}$ is the maximum deformation amplitude and L_b is the chord length of fish body.

The maximum deformation amplitude curves of caudal peduncle under various s and ε are shown in Figure 2.

The motion equations at the end of caudal peduncle could be deduced from (1), as follows:

$$A(t) = A\left[\frac{s-3}{3(s-1)}\right]^{\varepsilon} \sin(2\pi f t) \quad s > 3,\ \varepsilon > 1,$$

$$\beta(t) = \arctan\left\{A\frac{s}{s-1}\left[\frac{s-3}{3(s-1)}\right]^{\varepsilon-1} \sin(2\pi f t)\right\} \quad s > 3,\ \varepsilon > 1. \tag{3}$$

Additionally, (3) described the transverse motion of caudal fin. The following assumptions were made that the rigid caudal fin oscillated equally around the end of caudal peduncle with the same frequency as flexible deformation in caudal peduncle but having certain phase difference. So the oscillation equation of caudal fin could be deduced as follows:

$$\theta(t) = \theta_{\max} \sin(2\pi f t + \varphi), \tag{4}$$

where $\theta(t)$ is the oscillation angle, $\theta_{\max}$ is the maximum oscillation amplitude, and φ is the phase difference between transverse motion and rigid oscillation.

Then the attack angle of caudal fin could be deduced as follows:

$$\alpha(t) = \beta(t) + \theta(t). \tag{5}$$

2.2. Numerical Method. The Panel method based on perturbation potential was applied to the hydrodynamics analysis of bionic hydrofoil. The fluid around the hydrofoil was assumed to be irrotational, incompressible, and inviscid; then the perturbation potential, $\phi(t)$, can be deduced to satisfy the Laplace equation, as follows:

$$\nabla^2\phi(t) = 0. \tag{6}$$

At the trailing edge of caudal fin, $\phi(t)$ satisfied the Kutta condition, as follows:

$$|\nabla\phi(t)| < \infty. \tag{7}$$

The following equation could be deduced according to the no-penetrate principle on the surface of fish, as follows:

$$\frac{\partial\phi(t)}{\partial n_b} = -\mathbf{V}(\mathbf{t}) \cdot \mathbf{n_b}, \tag{8}$$

where $\partial/\partial n_b$ is the normal derivative on the surface and $\mathbf{V(t)}$ is the speed of fluid element on the surface, as follows:

$$\mathbf{V}(\mathbf{t}) = \mathbf{V_0} + \mathbf{V_p} + \mathbf{V_q}, \tag{9}$$

where $\mathbf{V_0}$ is the inflow velocity, $\mathbf{V_p}$ is the induction velocity produced by the deformation of caudal peduncle, and $\mathbf{V_q}$ is the pulling speed produced by the oscillation of caudal fin. $\mathbf{V_p}$ and $\mathbf{V_q}$ are available by solving (1)~(4).

The pressure distribution on fish body surface was available according to the Bernoulli equation, as follows:

$$p(t) = p_0 + \frac{1}{2}\rho\left[|\mathbf{V_0}|^2 - |\mathbf{V}(\mathbf{t})|^2\right] - \rho\frac{\partial\phi(t)}{\partial t}. \tag{10}$$

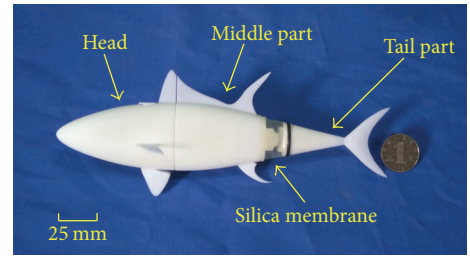

Figure 3: Physical prototype.

The hydrodynamic coefficients (propulsive force coefficient C_d, lateral force coefficient C_l, and pitching moment coefficient C_m) can be calculated by the following equations, as follows:

$$C_d = \int \frac{p(t)}{0.5\rho|\mathbf{V}(\mathbf{t})|^2 L} n_x dl,$$

$$C_l = \int \frac{p(t)}{0.5\rho|\mathbf{V}(\mathbf{t})|^2 L} n_y dl, \tag{11}$$

$$C_m = \int \frac{p(t)}{0.5\rho|\mathbf{V}(\mathbf{t})|^2 L^2} (xn_y - yn_x)\, dl,$$

where ρ is the fluid density and L is the characteristic chord length.

3. Verification and Numerical Simulation

3.1. Experimental Model. The physical prototype to mimic the shape of tuna was developed with the revolutionized technology of rapid prototyping manufacturing conveniently, as shown in Figure 3. The total length of the robofish was 209 mm and the main material was photosensitive resin. The middle part and the tail part were connected with silica membrane to keep watertight. A transmission mechanism was implemented into the inner middle part and a micro servomotor was utilized to drive it. The tail part would oscillate rigidly in varied frequency by controlling rotation rate of the servomotor and the oscillation amplitude could reach to 45°.

Besides, force sensors and signal acquisition module were used to test and record the hydrodynamic force of robofish swimming in water, as shown in Figure 4. The sampling frequency of signal acquisition module was set as 0.1 s.

3.2. Verification of Numerical Method. The vortex lattice method, a kind of Panel method, was applied to solve hydrodynamic coefficients numerically. In the computation process, induction velocity was calculated by Biot-Savart formula, as (12), and the iterative computation was controlled by Gauss-Seidel method,

$$dv = \frac{\Gamma}{4\pi}\frac{r \cdot dl}{r^3}. \tag{12}$$

To verify the numerical computation method utilized in studying rigid oscillation of hydrofoil, the NACA0012 aerofoil

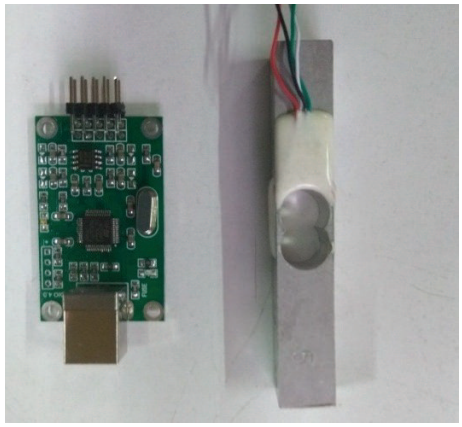

Figure 4: Force sensor and signal acquisition module.

was selected and the following parameters were set as follows: oscillation amplitude $\theta_{\max} = 45^\circ$, oscillation frequency $f = 0.5$ Hz, phase difference $\varphi = 0^\circ$, and inflow velocity $V_0 = 5L_b$ m/s.

Meanwhile, simulation on the rigid oscillation of hydrofoil was conducted with the commercial software *Fluent*. The turbulence model was set as k-ε model and the calculation method was selected as pressure-velocity coupling SIMPLE method. To ensure the simulation precision, the momentum equation was dispersed with second-order upwind scheme while the turbulent kinetic energy equation and the turbulent dissipation rate equation were dispersed with first-order upwind scheme.

On the other hand, the physical prototype was used as an added validation and the tail part was controlled to oscillate in 0.5 Hz.

The results of lateral force coefficient and pitching moment coefficient calculated by the numerical method and the commercial software *Fluent* are shown in Figure 5, as well as the results based on the experimental data.

As shown in Figure 5, the hydrodynamic coefficients calculated by the numerical method have good coherence with those of the commercial software *Fluent* and the experimental data. The hydrofoil thickness is ignored in Panel method, so the hydrodynamic coefficients are a little smaller than the results from *Fluent* and the change curves lag somewhat behind those from *Fluent*. Besides, the manufacturing precision of physical prototype and the three-dimensional effect are the key factors for the differences from experimental data. The numerical method derived in the front part of this paper is verified by the commercial software *Fluent* and the experimental data, and this method will be used to analyze the hydrodynamic performance of the coupled hydrofoil which consisted of flexible deformation hydrofoil and rigid oscillating hydrofoil in the following part of this paper.

3.3. Numerical Analysis of Coupled Hydrofoil. The method mentioned above was utilized in analyzing the hydrodynamic performance of coupled hydrofoil which consisted of flexible caudal peduncle and rigid caudal fin. In the calculation process, s, ε, and φ were taken into consideration specially.

Table 1: Parameters values.

Number	s	ε	φ
1	5	1	0°
2	12	1.5	45°
3	20	2	90°
4	1000	4	135°

The value of s was selected from 5, 12, 20, and 1000, the value of ε was selected from 1, 1.5, 2, and 4, and the value of φ was selected from 0°, 45°, 90°, and 135°, as shown in Table 1. To find out the optimal combination of s, ε, and φ, a three-factor and four-level orthogonal experiment was designed and the parameters were arranged following the orthogonal table $L_{16}(4^3)$.

The fish-like deformation is shown in Figure 6 under various values of s, ε, and φ.

In the calculation process, the following parameters were set as follows: chord length of caudal fin $L_f = 0.3L_b$, maximum deformation amplitude $A_{\max} = 0.2L_b$, oscillation amplitude of caudal fin $\theta_{\max} = 45^\circ$, deformation frequency and oscillation frequency were the same value as $f = 0.5$ Hz, and inflow velocity $V_0 = 5L_b$ m/s. The relationship between propulsive force D and propulsive force coefficient C_d is shown in (13) while the relationship between lateral force T and lateral force coefficient C_l is shown in (14) as follows:

$$C_d = \frac{D}{0.5\rho V^2 L}, \tag{13}$$

$$C_l = \frac{T}{0.5\rho V^2 L}. \tag{14}$$

The propulsive force and lateral force were averaged over a cycle time, and the resultant propulsive force and propulsive efficiency can be calculated, as shown in Table 2.

The Extremum Difference Analysis Method which would catch valuable results with a small number of data was applied to analyze the calculation results. K and R of single index analysis for propulsive force are shown in Table 3.

As shown in Table 3, the optimal values of various factors are s_1 ($s = 5$), ε_4 ($\varepsilon = 4$), and φ_1 ($\varphi = 0^\circ$), which is the optimal combination taken propulsive force as analysis index. Meanwhile, what matters most to the propulsive force is the phase difference between transverse motion and rigid oscillation, φ.

K and R of single index analysis for propulsive efficient are shown in Table 4.

As shown in Table 4, the optimal values of various factors are s_2 ($s = 12$), ε_1 ($\varepsilon = 1$), and φ_3 ($\varphi = 90^\circ$), which is the optimal combination taken propulsive efficient as analysis index, and the most influential factor is φ as well.

The calculated K and R with comprehensive consideration of propulsive force and propulsive efficient are shown in Table 5.

It is more intuitive to show the influence of various factors on propulsive force and propulsive efficient in Figure 7.

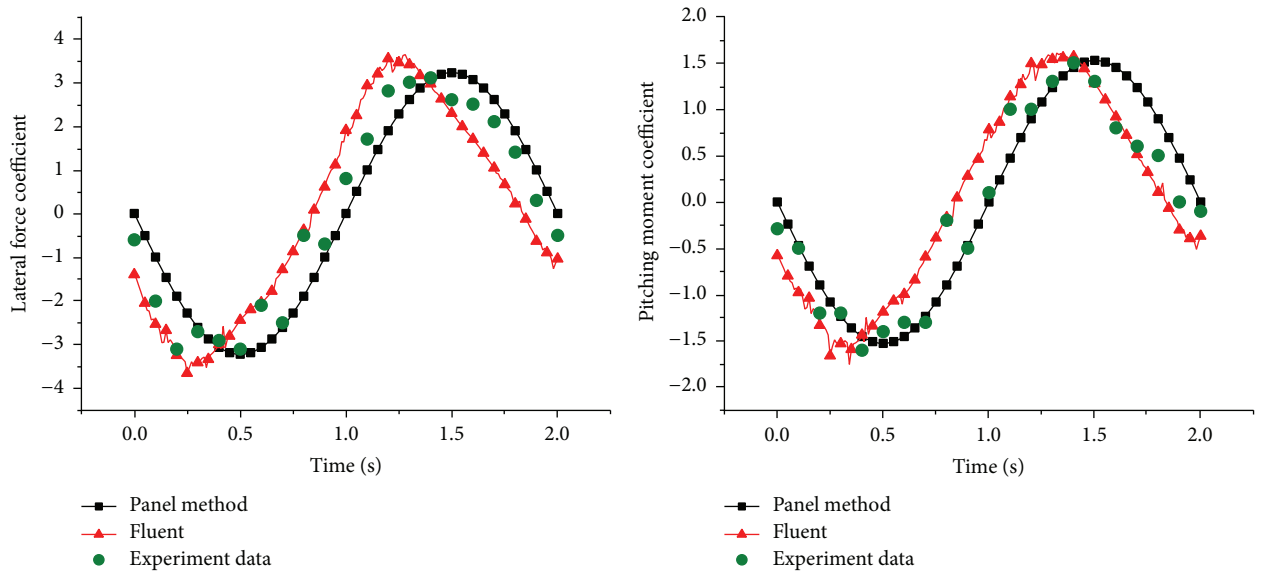

Figure 5: Hydrodynamic coefficients of the caudal fin with rigid swing.

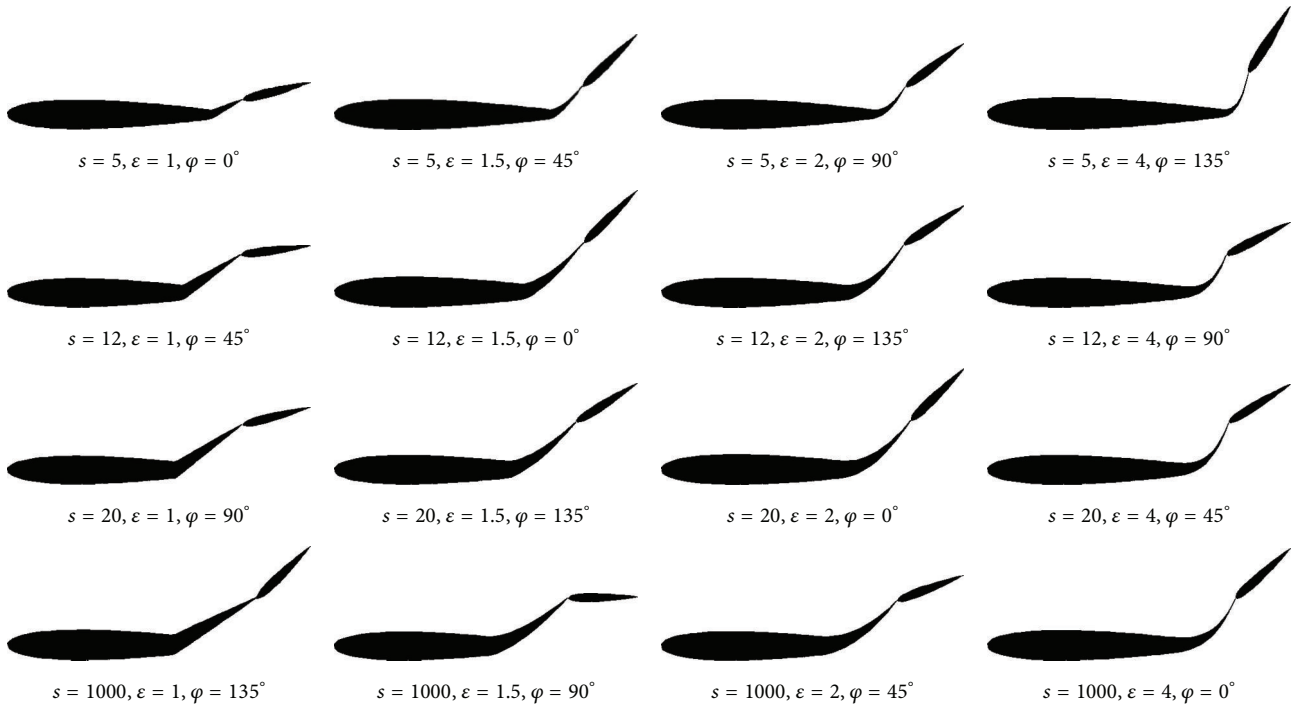

Figure 6: Fish-like deformation under various s, ε, and φ.

As shown in Figure 7, the function of φ_1 in improving propulsive force is much more remarkable than that of φ_3 in improving propulsive efficient, the effect of s_2 on promoting propulsive efficient is more obvious than that of s_1 on promoting propulsive force, and the impact of ε_4 on enhancing propulsive force is a little more effective than that of ε_1 on enhancing propulsive efficient. Accordingly, the optimal combination with comprehensive consideration of propulsive force and propulsive efficient is $\varphi_1 s_2 \varepsilon_4$, and the corresponding values are $s = 12$, $\varepsilon = 4$, and $\varphi = 0^\circ$.

3.4. Simulation on Optimal Combination. The hydrodynamic performance curves were further analyzed for the optimal combination as $s = 12$, $\varepsilon = 4$, and $\varphi = 0^\circ$ by the commercial software *Fluent* to verify the optimal results. Corresponding parameters were similar to that in Section 3.2. In a fish motion cycle, the curves of hydrodynamic force varied with time are shown in Figure 8.

According to the simulation for the optimal combination, the average resultant propulsive force can be 30.573 N and the propulsive effective will reach to 98.35%, which represents an

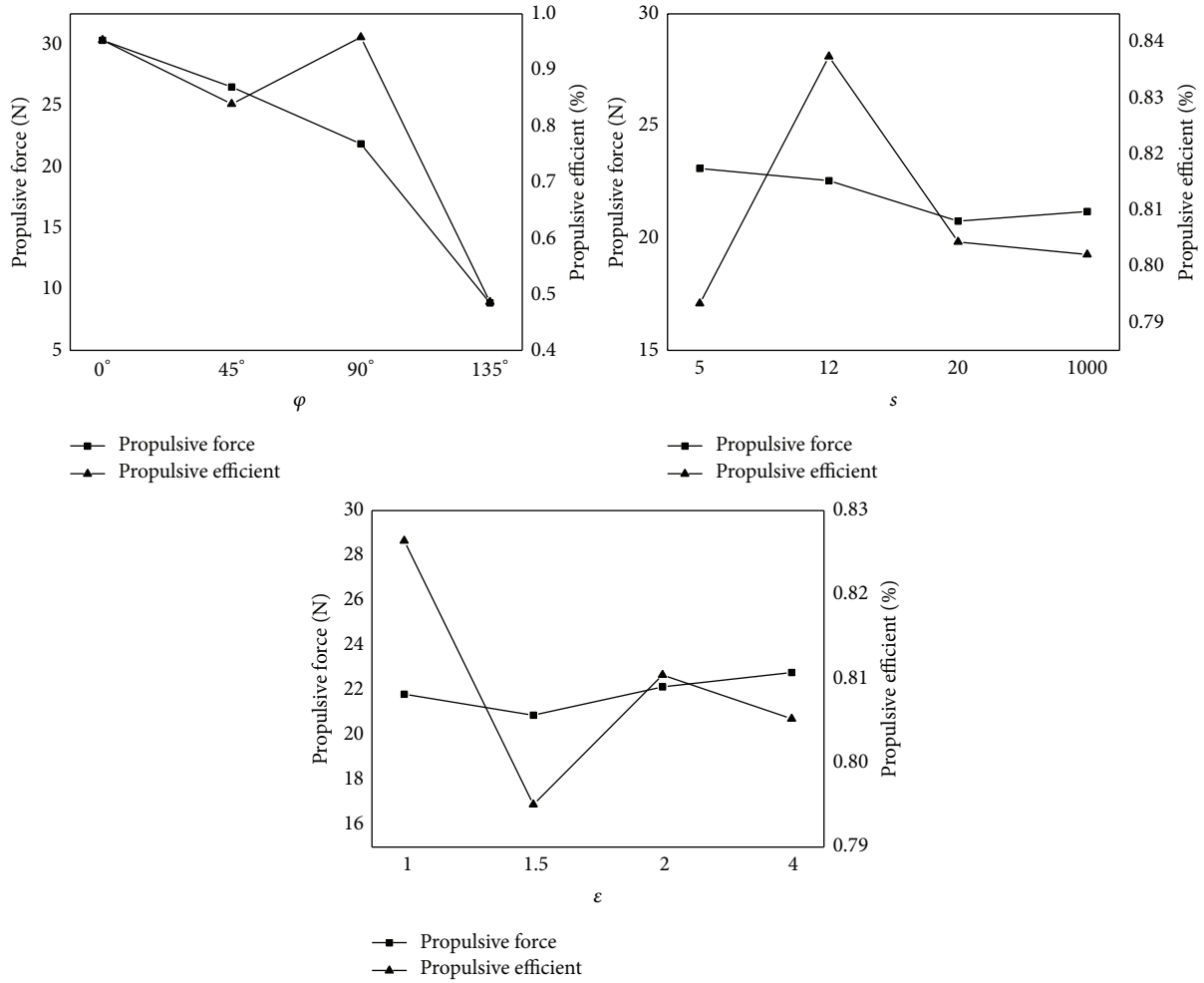

Figure 7: Influences on propulsive force and propulsive efficiency of different parameters.

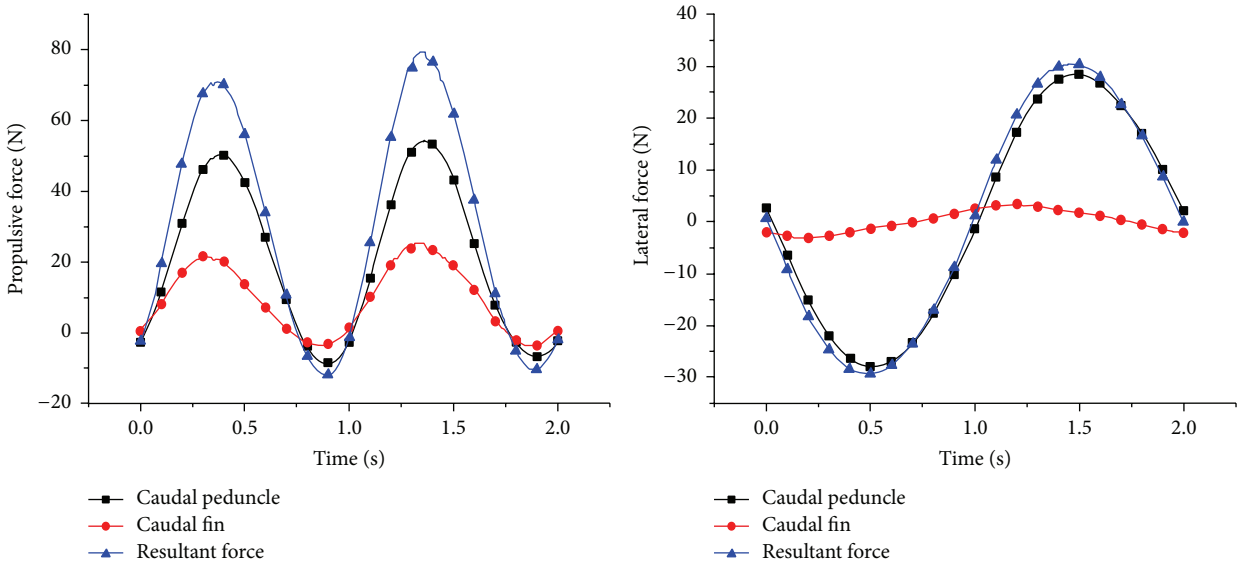

Figure 8: Hydrodynamic curves for the optimal parameters combination.

Table 2: Results of numerical computation.

Number	s	ε	φ	Caudal peduncle		Caudal fin		Resultant propulsive force (N)	Propulsive efficiency
				Averaged propulsive force (N)	Averaged lateral force (N)	Averaged propulsive force (N)	Averaged lateral force (N)		
1	5	1	0°	19.675	−2.85	12.25	0.6925	31.925	93.67%
2	5	1.5	45°	18.8	8.05	7.475	0.01465	26.275	78.81%
3	5	2	90°	13.15	0.4725	10.325	1.1625	23.475	93.49%
4	5	4	135°	5.225	−5.625	5.55	−4.575	10.775	51.37%
5	12	1	45°	17.7	3.55	9.7	−1.135	27.4	91.9%
6	12	1.5	0°	19.3	0.6925	10.325	0.1875	29.625	97.12%
7	12	2	135°	4.95	−5.15	4.475	−4.525	9.425	49.35%
8	12	4	90°	12.95	−0.22675	10.85	1.0675	23.8	96.59%
9	20	1	90°	7.625	−1.605	12.125	1.2575	19.745	98.27%
10	20	1.5	135°	4.3	−3.975	2.825	−4.025	7.125	47.11%
11	20	2	0°	19.55	−1.3075	10.15	0.17775	29.7	96.34%
12	20	4	45°	19.15	−7.15	7.325	0.03625	26.475	80.01%
13	1000	1	135°	4.175	−4.575	4.025	−4.775	8.2	46.72%
14	1000	1.5	90°	7.925	−2.195	12.575	1.1125	20.5	94.98%
15	1000	2	45°	17.325	−4.45	8.65	−0.13525	25.975	85%
16	1000	4	0°	20.425	−1.98	9.65	0.1045	30.075	94.13%

Table 3: K and R for propulsive force.

	s	ε	φ
$K1$	23.1125	21.8175	30.33125
$K2$	22.5625	20.88125	26.53125
$K3$	20.76125	22.14375	21.88
$K4$	21.1875	22.78125	8.88125
R	2.35125	1.9	21.44875

Table 4: K and R for propulsive efficiency.

	s	ε	φ
$K1$	79.335%	82.64%	95.315%
$K2$	83.74%	79.505%	83.93%
$K3$	80.4325%	81.045%	95.8325%
$K4$	80.2075%	80.525%	48.6375%
R	4.405%	3.135%	46.6775%

Table 5: K and R for propulsive force and propulsive efficiency.

Index	Importance order	Optimal combination
Propulsive force	$\varphi s\varepsilon$	$\varphi_1 s_1 \varepsilon_4$
Propulsive efficient	$\varphi s\varepsilon$	$\varphi_3 s_2 \varepsilon_1$

outstanding overall performance. The integral value of lateral force in a motion cycle tends to zero, which demonstrates fish swimming method having a high average propulsive efficient. Besides, we used a 4D figure to show the results directly based on the data from Table 2 and the simulation for optimal combination, as shown in Figure 9.

In Figure 9, x-axis, y-axis, and z-axis represent s, ε, and φ, respectively. The volume of each ball represents value of propulsive force or propulsive efficient. The two black balls have the same volume to play the role of reference substance and the two blue balls represent the results of optimal combination. It is obvious that φ has a more remarkable efficient on propulsive force than that on propulsive efficient. The two black balls are both in large scale for the two figures, which verifies the optimal results.

According to the results of numerical analysis, the value of s, which controls the oscillation range of caudal peduncle, getting larger will result in the initial oscillation position moving closer to the point at two-thirds of the fish body. When the oscillation range of caudal peduncle is small, the propulsive force is small, but the propulsive efficient is high. As $s = 12$, the initial oscillation position of caudal peduncle is near to the point at two-thirds of the fish body relatively; the values of propulsive force and propulsive efficient are both at high level. ε controls the deformation flexibility of caudal peduncle. As $\varepsilon = 4$, the caudal peduncle oscillates flexibly to produce a comparatively high propulsive force but a quite small drag force, so the propulsive efficient is somewhat high. The propulsive force will have a considerable promotion by increasing the deformation flexibility of caudal peduncle but no significant decline happens in propulsive efficient. When φ is equal to 0° or 90°, the propulsive efficient is at a high level but the propulsive force decreases dramatically as φ getting larger.

4. Wake Field Analysis

The phase difference between transverse motion and rigid oscillation of caudal fin is the key factor to propulsive force and propulsive efficient. Furthermore, the distribution of trailing vortex was analyzed under various φ, as shown from Figures 10–12.

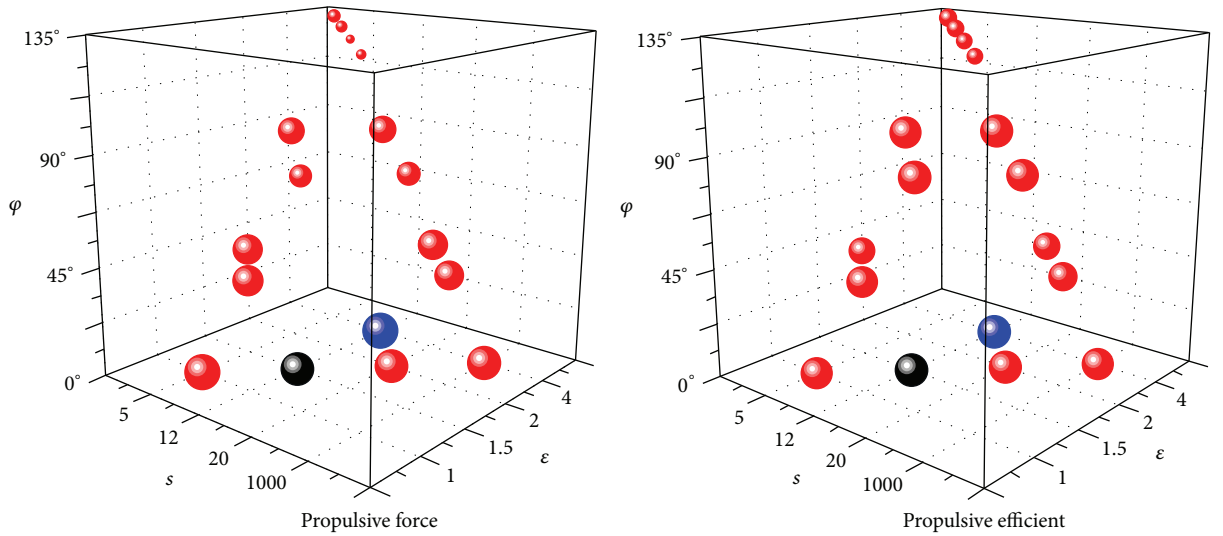

Figure 9: Influences of various φ, s, and ε.

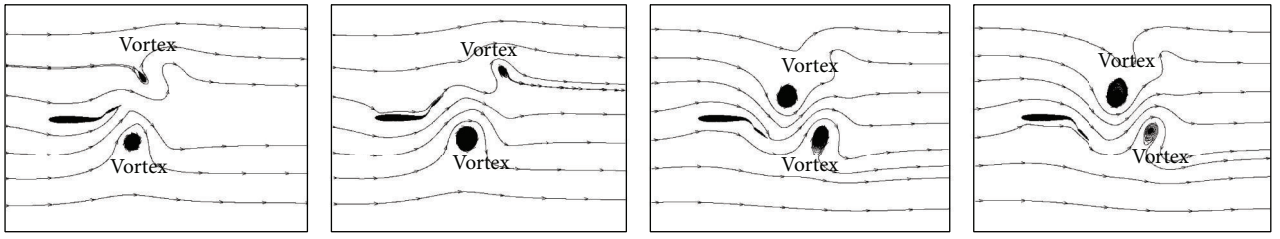

$t = 0.25\,s$ $t = 0.5\,s$ $t = 1.25\,s$ $t = 1.5\,s$

Figure 10: Trailing vortex at $\varphi = 0^{\circ}$.

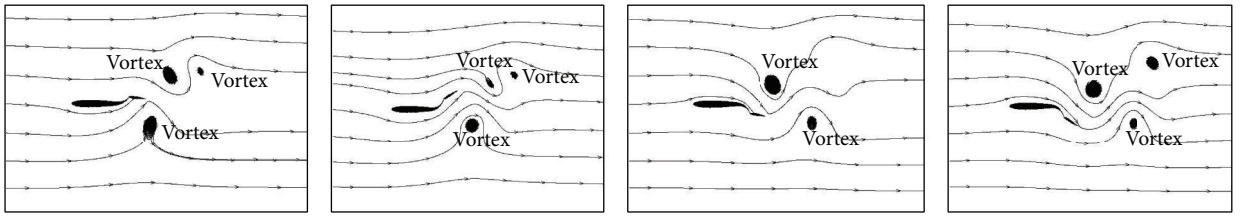

$t = 0.25\,s$ $t = 0.5\,s$ $t = 1.25\,s$ $t = 1.5\,s$

Figure 11: Trailing vortex at $\varphi = 45^{\circ}$.

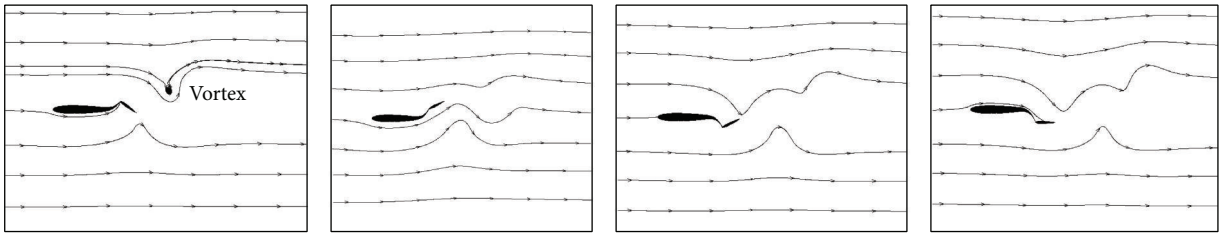

$t = 0.25\,s$ $t = 0.5\,s$ $t = 1.25\,s$ $t = 1.5\,s$

Figure 12: Trailing vortex at $\varphi = 90^{\circ}$.

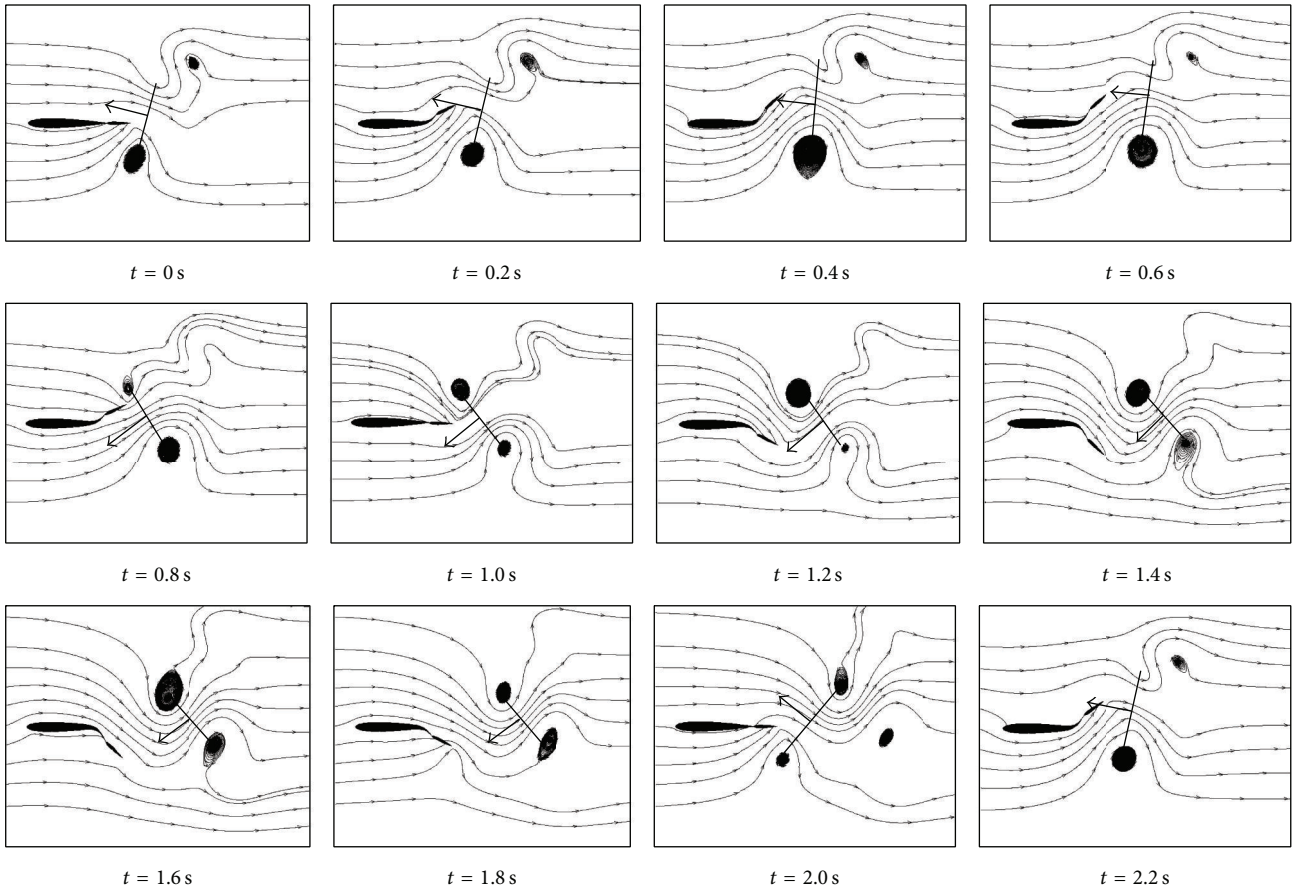

Figure 13: Trailing vortex for the optimal parameters combination.

As $\varphi = 0^{\circ}$, the strength of reversed Kaman vortex street generated in the wake filed is quite large, which leads to the huge propulsive force. As $\varphi = 45^{\circ}$, the reversed Kaman vortex street to generate propulsive force and the Kaman vortex street to generate drag force are both obvious in the wake field, and the interaction decreases the propulsive force and the propulsive efficient. As $\varphi = 90^{\circ}$, no distinct reversed Kaman vortex street is generated in the wake filed and the propulsive force is relatively small. Figures 10–12 show good coherence with above results of numerical calculation.

In the numerical calculation, the inflow velocity was set as $V_0 = 5L_b$ m/s, so the downwash velocity near caudal peduncle and caudal fin was relatively small. As Figures 10–12 shown, the vortex is generated at the end of caudal peduncle, sheds along the caudal fin, and dissipates quickly in the wake field. However, the phase difference between caudal peduncle motion and caudal fin motion is the key factor to influence the vortex shedding. It is quite obvious that the shape of trailing vortex is similar to the image of motion curve at the trailing edge when $\varphi = 90^{\circ}$, as shown in Figure 12, which verifies the correctness of linear vortex plane assumption.

The wake field structure was further analyzed for the optimal combination as $s = 12$, $\varepsilon = 4$, and $\varphi = 0^{\circ}$ to expound the fish swimming mechanism in the respect of function from trailing vortex. Taking arbitrary time of the fish motion as initial moment and the wake field structures in 2.2 s (about one cycle) are shown in Figure 13.

As shown in Figure 13, paired reversed Kaman vortex streets are generated in the wake filed to result in acceleration of fluid flowing and generation of jet function. The reactive force of jet fluid goes in opposite direction of streamline and acts on the fish body, as the arrows shown in Figure 13. At the initial moment, the fish keeps still, the body goes along the streamline, and the acting force of trailing vortex goes along the fish body nearly. Thus propulsive force and lateral force are really small, tending to zero, which agrees with the hydrodynamic performance values in Figure 8. As the deformation and oscillation starting, a certain angle between trunk line and streamline is generated, which leads to the drag force along inflow direction and the lateral force perpendicular to inflow direction. Meanwhile, the acting face is generated for the acting force from trailing vortex, and the acting force acts on the deformed caudal peduncle and caudal fin will balance out the drag force along inflow direction; thus certain propulsive force is generated. It is obvious in Figure 13 that the acting face and strength of trailing vortex reach to a high level from 0.4 s to 0.6 s and from 1.4 s to 1.6 s. So the trailing vortex has more significant effect on fish during this period, which is in line with propulsive force reaching to the maximum value shown in Figure 8 at 0.5 s and 1.5 s.

It is not hard to see from Figure 13 that the inflow water strikes on caudal peduncle directly because of deformation motion to generate a huge lateral force on caudal peduncle and no corresponding force perpendicular to inflow direction to offset it, which leads to a relative huge lateral force. It is because of the coupled hydrofoil which consisted of flexible caudal peduncle and rigid caudal fin that the deformed caudal peduncle plays the role of flow guider to make water flow along caudal fin. Then the actual attack angle of caudal fin nearly equals zero to make the lateral force small, so the propulsive efficient is at a high level, which is in line with the results in Figure 8 as well.

5. Conclusion

The carangiform propulsion mode was established numerically based on the Slender-Body theory according to fish swimming feature. Various motion states were achieved by controlling s, ε, and φ to simulate the motion of fish adequately. The Panel method was applied to analyze hydrodynamic performance of rigid oscillating hydrofoil, and the results were compared with those from the commercial software *Fluent* and the experimental data from the robofish to prove rationality and validity of the numerical method. Furthermore, the hydrodynamic performance of coupled hydrofoil which consisted of flexible fish body and rigid caudal fin was calculated numerically. The results showed that the small deformation range of caudal peduncle would lead to a high propulsive efficient but a small propulsive force. The propulsive efficient would be improved by increasing deformation flexibility of caudal peduncle and no obvious decrease happened in propulsive force. The propulsive force would have an apparent decline when increasing the phase angle. The multifactor and multilevel calculation results were analyzed by Orthogonal Experimental Method to find out the optimal parameters combination, which had some reference values to design and optimization of bionic underwater vehicle.

Furthermore, the phase difference between flexible deformation of caudal peduncle and rigid oscillation of caudal fin was analyzed deeply according to the wake field structure. It can be seen from the hydrodynamic performance curves and wake field structures that phase angle was the key factor to influence hydrodynamic performance of swimming motion and had an effect on trailing vortex shedding. When the downwash velocity was small, the shape of trailing vortex was similar to the image of the motion curve at the trailing edge. The reversed Kaman vortex street, a kind of propulsive trailing vortex, was available at certain phase angles. The hydrodynamic performance and function mechanism of trailing vortex were analyzed for the optimal combination to find that the strength and acting face of trailing vortex were both huge to generate a relative large propulsive force when the deformation amplitude was large and the phase angle tended to zero. The numerical research may have certain value to reveal the fish swimming mechanism.

Competing Interests

The authors declare that there are no competing interests regarding the publication of this paper.

Acknowledgments

The research was supported by the front and emerging discipline team oriented project of Shandong University Marine Resources and Utilization of Key Scientific Research (Project no. 2014QY006) and The Fundamental Research Funds of Shandong University (Project no. 2016JC035), which are gratefully acknowledged.

References

[1] J. Wu, "Double-vortex structure of fish oscillating propulsion and relative experimental study," *Journal of Beijing University of Aeronautics and Astronautics*, vol. 20, no. 2, pp. 158–163, 1994.

[2] J. Katz and D. Weihs, "Hydrodynamic propulsion by large amplitude oscillation of an airfoil with chordwise flexibility," *Journal of Fluid Mechanics*, vol. 88, no. 3, pp. 485–497, 1978.

[3] M. S. Triantafyllou, D. S. Barrett, D. K. P. Yue et al., "A new paradigm of propulsion and maneuvering for marine vehicles," *Transactions of the Society of Naval Architects and Marine Engineers*, vol. 104, pp. 81–100, 1996.

[4] R. Du, Z. Li, K. Youcef-Toumi, and P. Valdivia y Alvarado, *Robot Fish: Bio-Inspired Fishlike Underwater Robots*, Springer Tracts in Mechanical Engineering, Springer, New York, NY, USA, 2015.

[5] S.-Y. Wang, J. Zhu, X.-G. Wang, Q.-F. Li, and H.-Y. Zhu, "Kinematics modeling and simulation of a bionic fish tail system based on linear hypocycloid," *Applied Bionics and Biomechanics*, vol. 2015, Article ID 697140, 8 pages, 2015.

[6] Q. Wu, G. Y. Wang, and B. Huang, "Numerical methods and transition investigation of transient flows around a pitching hydrofoil," *Chinese Journal of Theoretical and Applied Mechanics*, vol. 46, no. 1, pp. 60–69, 2014.

[7] F. Celik, Y. Arikan Ozden, and S. Bal, "Numerical simulation of flow around two- and three-dimensional partially cavitating hydrofoils," *Ocean Engineering*, vol. 78, pp. 22–34, 2014.

[8] Y. Zhao, G. Y. Wang, B. Huang, Q. Wu, and F. F. Wang, "Lagrangian-based investigation of unsteady vertex structure near trailing edge of a hydrofoil," *Transactions of Beijing Institute of Technology*, vol. 35, no. 7, pp. 666–670, 2015.

[9] M. M. Karim, B. Prasad, and N. Rahman, "Numerical simulation of free surface water wave for the flow around NACA 0015 hydrofoil using the volume of fluid (VOF) method," *Ocean Engineering*, vol. 78, pp. 89–94, 2014.

[10] S. G. Shi, G. Y. Wang, and B. Huang, "The structure analysis about the cavitation flow around the cascade hydrofoil by numerical and experimental study," *Chinese Journal of Theoretical and Applied Mechanics*, vol. 43, no. 3, pp. 625–629, 2011.

[11] Q. Zhu, "Numerical simulation of a flapping foil with chordwise or spanwise flexibility," *AIAA Journal*, vol. 45, no. 10, pp. 2448–2457, 2007.

[12] H. X. Liu, Y. M. Su, X. Zhang, and S. Wang, "Effect of caudal-fin flexible deformation on self-propelled swimming of a tuna-like biomimetic underwater vehicle," *Journal of Huazhong University of Science and Technology (Natural Science Edition)*, vol. 42, no. 3, pp. 117–121, 2014.

[13] X. Zhang, Y. M. Su, and Z. L. Wang, "Hydrodynamic research on the effects of a chordwise deflection phase angle on a flexible caudal fin," *Journal of Harbin Engineering University*, vol. 32, no. 11, pp. 1402–1409, 2011.

[14] Y.-M. Su, H.-X. Liu, X. Zhang, and S. Wang, "Numerical research on the self-propelled swimming of a tunalike biomimetic underwater vehicle with flexible tail fin," *Journal of Ship Mechanics*, vol. 17, no. 5, pp. 468–477, 2013.

[15] A. Leroyer and M. Visonneau, "Biohydrodynamics and numerical simulations," *Houille Blanche*, no. 3, pp. 45–51, 2005.

[16] A. Leroyer and M. Visonneau, "Numerical methods for RANSE simulations of a self-propelled fish-like body," *Journal of Fluids and Structures*, vol. 20, no. 7, pp. 975–991, 2005.

[17] S.-J. Lee, J.-H. Lee, and J.-C. Suh, "Numerical investigation on vortex shedding from a hydrofoil with a beveled trailing edge," *Modelling and Simulation in Engineering*, vol. 2015, Article ID 565417, 13 pages, 2015.

[18] J. Lighthill, "Large-amplitude elongated-body theory of fish locomotion," *Proceedings of the Royal Society B: Biological Sciences*, vol. 179, no. 1055, pp. 125–138, 1971.